Electronic Supplementary Material (ESI) for Journal of Materials Chemistry A.

Supplementary Information

Spontaneous Enhancement of the Stable Power Conversion Efficiency in Perovskite Solar Cells

Somayeh Moghadamzadeh,*[ab] Ihteaz M. Hossain,[ab] Marius Jakoby,[ab] Bahram Abdollahi Nejand,[ab] Diana Rueda-Delgado,[b] Jonas A. Schwenzer,[b] Saba Gharibzadeh,[ab] Motiur Rahman Khan,[a] Tobias Abzieher,[b] Amir A. Haghighirad,[c] Ian A. Howard,[ab] Bryce S. Richards,[ab] Uli Lemmer,[abd] and Ulrich W. Paetzold*[ab]

[a]Light Technology Institute, Karlsruhe Institute of Technology, Engesserstrasse 13, 76131 Karlsruhe, Germany

[b]Institute of Microstructure Technology, Karlsruhe Institute of Technology, Hermann-von-Helmholtz-Platz 1, 76344 Eggenstein-Leopoldshafen, Germany

[c]Institute for Solid-State Physics, Karlsruhe Institute of Technology (KIT), Hermann-von-Helmholtz-Platz 1, D-76021 Eggenstein-Leopoldshafen, Germany

[d]InnovationLab GmbH, Speyererstrasse 4, 69115 Heidelberg, Germany

*somayeh.moghadamzadeh@kit.edu, ulrich.paetzold@kit.edu

Table of contents:

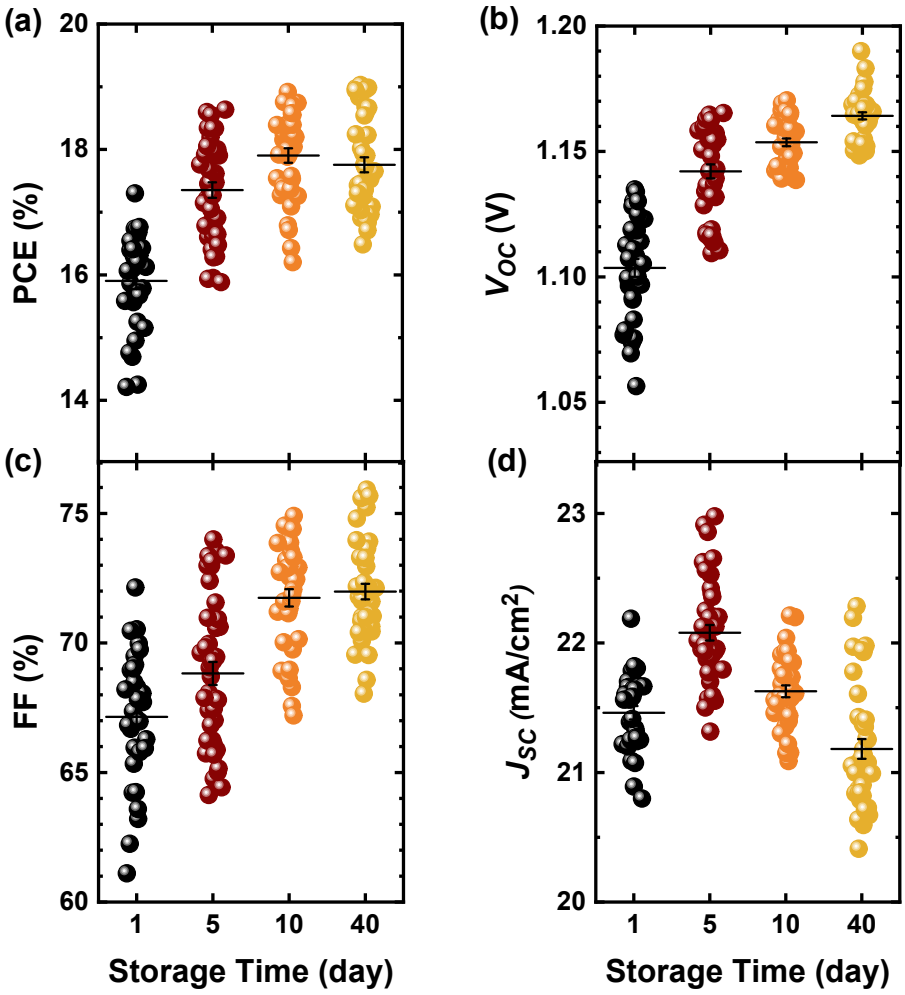

Fig. S1. Photovoltaic parameters of perovskite solar cells deposited on TiO_2 nanoparticles. (a) Power conversion efficiency (PCE), (b) open-circuit voltage (V_{OC}), (c) fill factor (FF), and (d) short-circuit current (J_{SC}), of 40 identically prepared $Cs_{0.1}(FA_{0.83}MA_{0.17})_{0.9}Pb(I_{0.87}Br_{0.13})_3$ solar cells measured on the day of samples preparation (day 1) and after storage (days 5, 10, and 40).

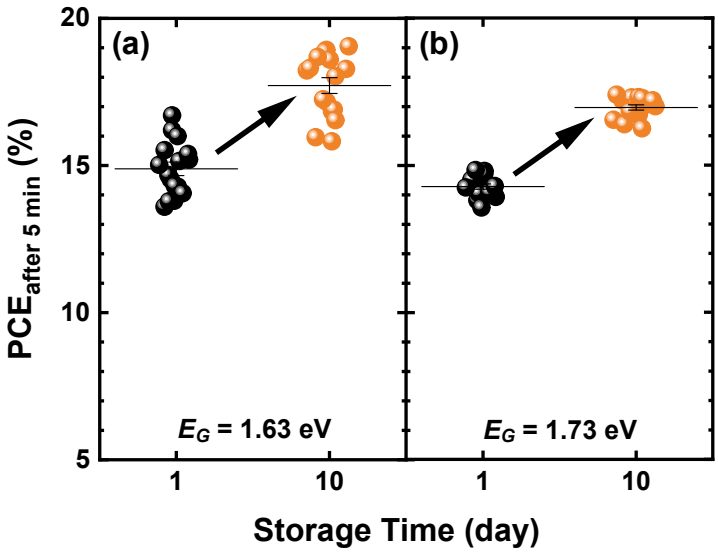

Fig. S2. Stable power conversion efficiency of perovskite solar cells with two different bandgaps. Stable power conversion efficiency after 5 min measured at constant voltage close to the maximum power point ($PCE_{after\ 5\ min}$), derived from 16 perovskite solar cells with perovskite thin film with the compositions (a) $Cs_{0.17}FA_{0.83}Pb(I_{0.83}Br_{0.17})_3$ with a bandgap of $E_G = 1.63$ eV, and (b) $Cs_{0.1}(FA_{0.83}MA_{0.17})_{0.9}Pb(I_{0.67}Br_{0.33})_3$ with a bandgap of $E_G = 1.73$ eV, measured on the day of samples preparation (day 1) and after storage (day 10).

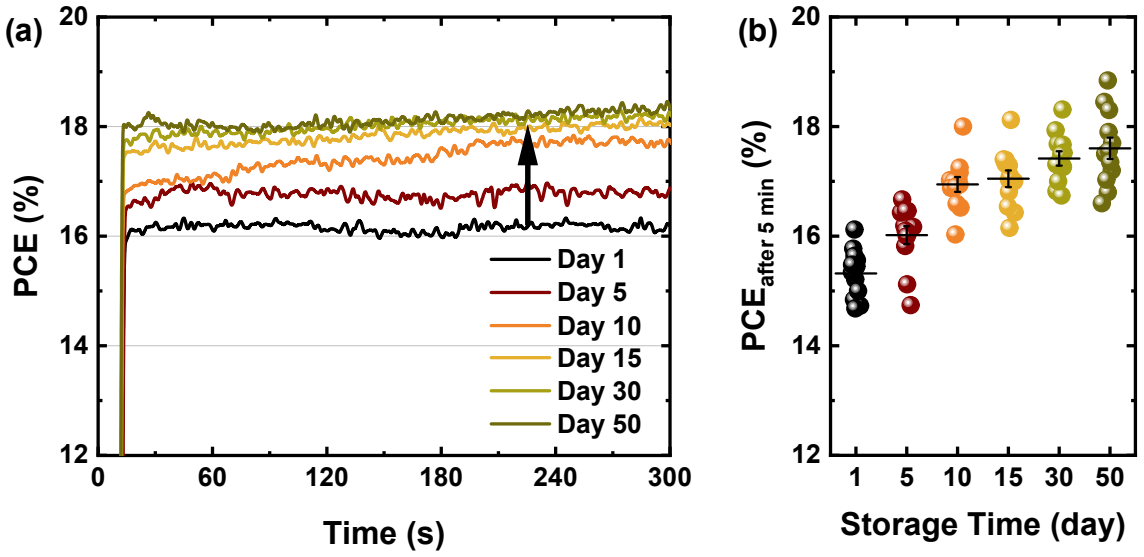

Fig. S3. Stable Power conversion efficiency of perovskite solar cells deposited on SnO_2 nanoparticles. (a) Stable Power conversion efficiency (PCE) measured for 300 s at constant voltage close to the maximum power point (MPP), derived from a $Cs_{0.1}(FA_{0.83}MA_{0.17})_{0.9}Pb(I_{0.83}Br_{0.17})_3$ solar cell ($Cs_{0.1}FM_{0.9}$). (b) Stable Power conversion efficiency after 5 min measured at constant voltage close to the MPP ($PCE_{after\ 5\ min}$), derived from 16 identically prepared $Cs_{0.1}FM_{0.9}$ solar cells deposited on SnO_2 nanoparticles, measured on the day of samples preparation (day 1) and after storage (days 5, 7, 15, 30, and 50), with the highest PCE of ~19% after 50 days for a champion solar cell.

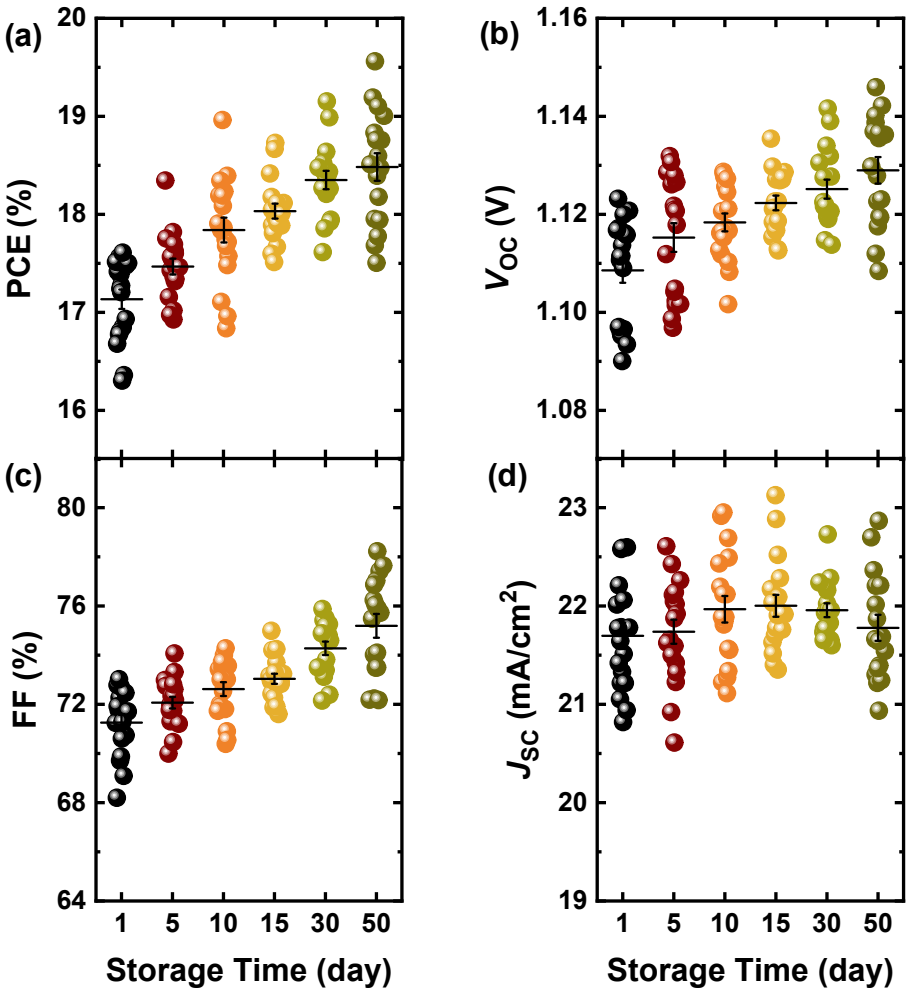

Fig. S4. Photovoltaic parameters of perovskite solar cells deposited on SnO_2 nanoparticles. (a) Power conversion efficiency (PCE) with the highest value of 19.6% after 50 days for a champion solar cell, (b) open-circuit voltage (V_{OC}), (c) fill factor (FF), and (d) short-circuit current (J_{SC}), of 40 identically prepared $Cs_{0.1}(FA_{0.83}MA_{0.17})_{0.9}Pb(I_{0.83}Br_{0.17})_3$ solar cells measured on the day of samples preparation (day 1) and after storage (days 5, 10, 15, 30, and 50).

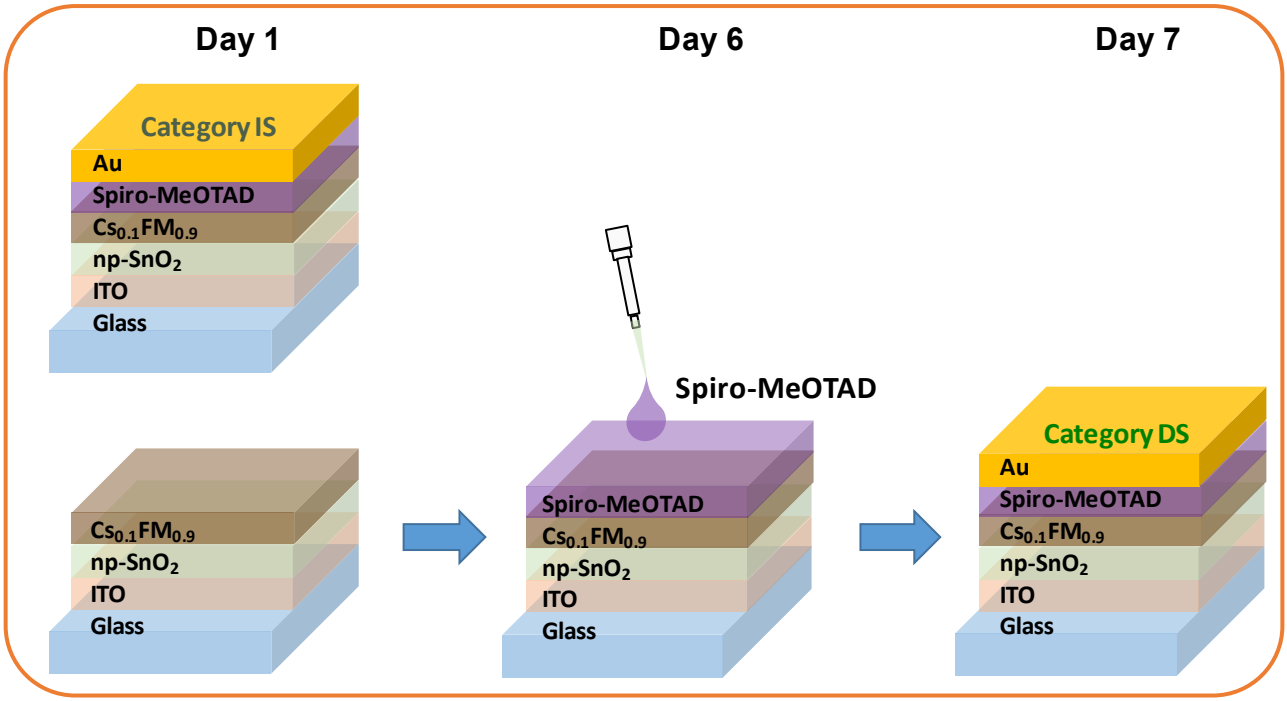

Fig. S5. Schematic illustration of device fabrication in terms of time interval between the deposition of the perovskite thin film and the deposition of spiro-MeOTAD as the hole transport layer. We complete the samples of category IS (immediate spiro-MeOTAD deposition) as usual on day 1. However, we complete the samples of category DS (delayed spiro-MeOTAD deposition) only up to perovskite layer on day 1 and store them in the dark in inert atmosphere with the samples IS. For these samples, the spiro-MeOTAD and gold are deposited on days 6 and 7 (after one night of oxygen doping), respectively.

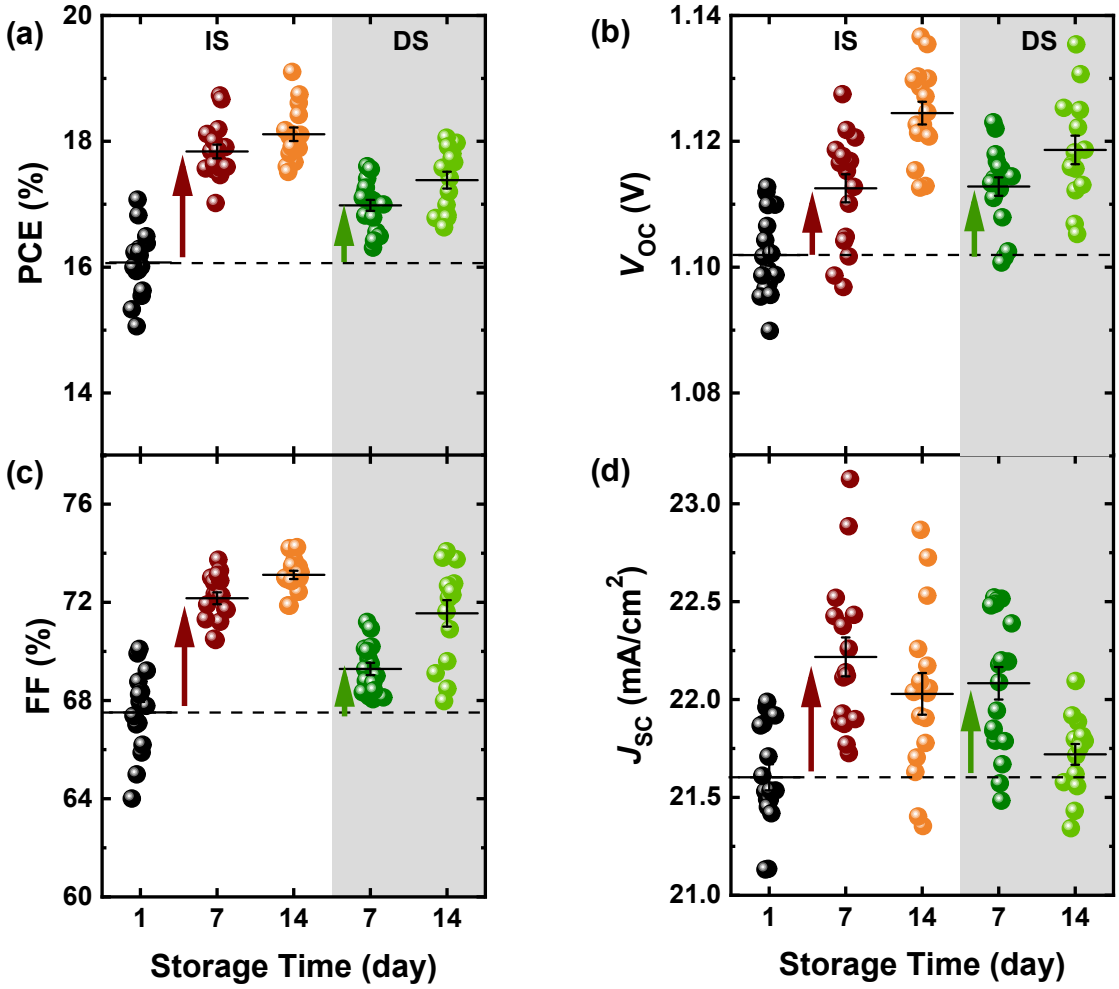

Fig. S6. Photovoltaic parameters of perovskite solar cells deposited on SnO_2 nanoparticles with: immediately deposited spiro-MeOTAD layers (IS) and delayed deposited spiro-MeOTAD layers (DS). (a) power conversion efficiency (PCE), (b) open-circuit voltage (V_{OC}), (c) fill factor (FF), and (d) short-circuit current (J_{SC}), of 16 $Cs_{0.1}(FA_{0.83}MA_{0.17})_{0.9}Pb(I_{0.83}Br_{0.17})_3$ solar cells of category IS (white background) and DS (gray background) measured on the day of samples preparation (day 1) and after storage (days 7 and 14).

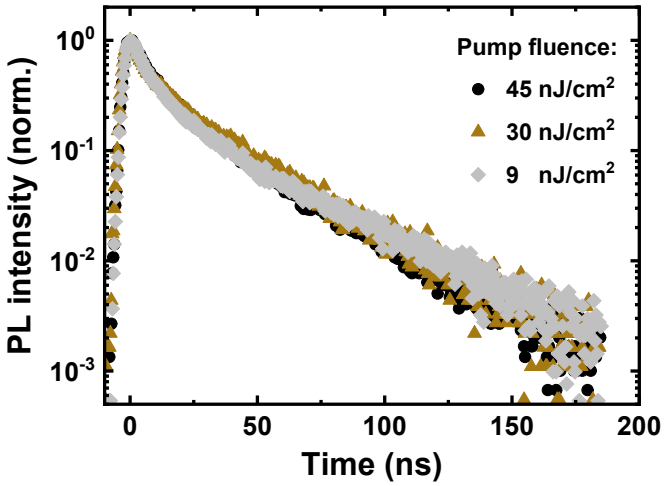

Fig. S7. Fluence-dependent time-resolved photoluminescence (PL) kinetics of a perovskite thin film deposited on bare glass for three different excitation fluences. Time-resolved PL of a $Cs_{0.1}(FA_{0.83}MA_{0.17})_{0.9}Pb(I_{0.83}Br_{0.17})_3$ thin film is independent of excitation fluences.

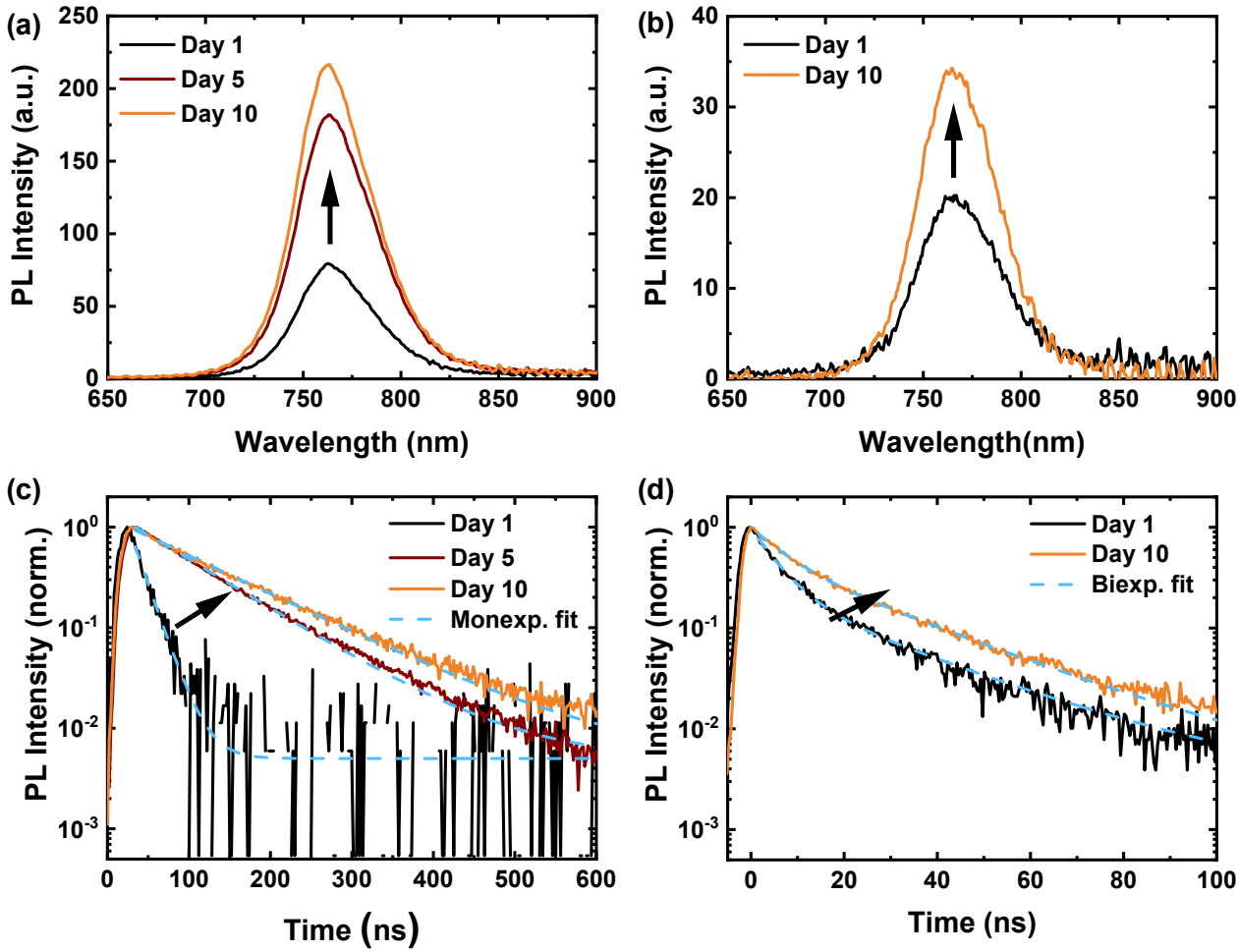

Fig. S8. Steady-state PL spectra and time-resolved PL kinetics of perovskite thin films. Top panels: steady-state PL spectra, and bottom panels: normalized time-resolved PL kinetics, derived from perovskite thin films with the composition $Cs_{0.1}(FA_{0.83}MA_{0.17})_{0.9}Pb(I_{0.83}Br_{0.17})_3$ deposited on glass/ITO/TiO_2 nanoparticles (a and c) and glass/ITO/SnO_2 nanoparticles (b and d), respectively. The data are collected on the day of samples preparation (day 1) and after storage (days 5 and 10).

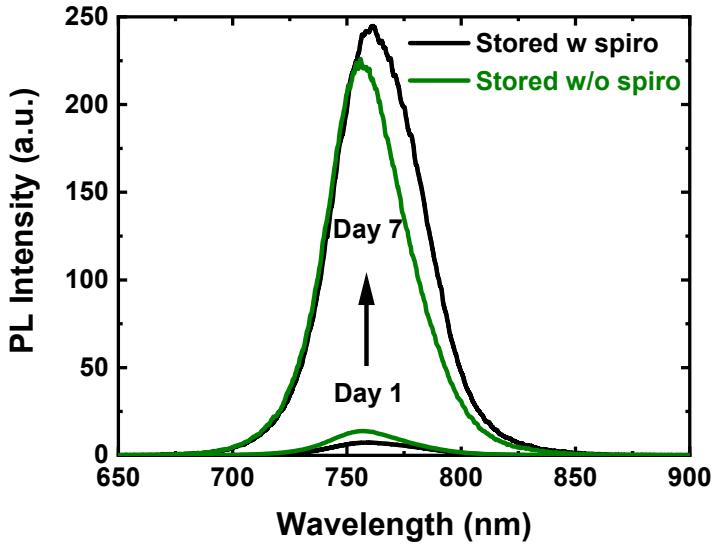

Fig. S9. Steady-state PL spectra of the perovskite thin films stored with and without spiro-MeOTAD. Steady-state PL of the $Cs_{0.1}(FA_{0.83}MA_{0.17})_{0.9}Pb(I_{0.83}Br_{0.17})_3$ thin films stored with and without spiro-MeOTAD are comparable on the day of samples preparation (day 1) and after storage (day 7). We use 0.15 ml chlorobenzene to wash the spiro-MeOTAD layer off the sample before the characterization.

Pseudo-Voigt Profile:

We carry out the fitting computation for the delayed PL spectra on days 1 and 10 (Fig. 7) using pseudo-Voigt function which is a linear contribution from both Gaussian and Lorentzian components. We define the following fitting equation - in Origin (version: 2018b 9.55) - for two bands:

$$f(x;A_1,X_{c1},w_1,\mu_1,A_2,X_{c2},w_2,\mu_2) =$$

$$A_1\left[\mu_1\frac{2}{\pi}\frac{w_2}{4\,(x-X_{c1})^2+{w_1}^2}+(1-\mu_1)\frac{\sqrt{4\ln(2)}}{\sqrt{\pi}\,w_1}e^{\frac{-4\ln(2)}{w_1^2}(x-X_{c1})^2}\right]+$$

$$A_2\left[\mu_2\frac{2}{\pi}\frac{w_2}{4\,(x-X_{c2})^2+{w_2}^2}+(1-\mu_2)\frac{\sqrt{4\ln(2)}}{\sqrt{\pi}\,w_2}e^{\frac{-4\ln(2)}{w_2^2}(x-X_{c2})^2}\right] \quad \text{(S1)}$$

in which x is energy in eV, A_1 and A_2 are the amplitudes, X_{c1} and X_{c2} are the center positions, and w_1 and w_2 are the FWHM of the two bands. $0 \le \mu_1 \le 1$ and $0 \le \mu_2 \le 1$ are the fractions of Lorentzian profiles in the function, such that if μ equals one the band is pure Lorentzian and if it equals zero the band is pure Gaussian.

Table S1. Relative (R.) area under PL peaks extracted from the fitting analysis of the PL spectra on days 1 and 10.

Storage Time	Day 1	Day 10
R. Area$_{(1.54\ eV)}$	81641	15260
R. Area$_{(1.62\ eV)}$	41820	56353

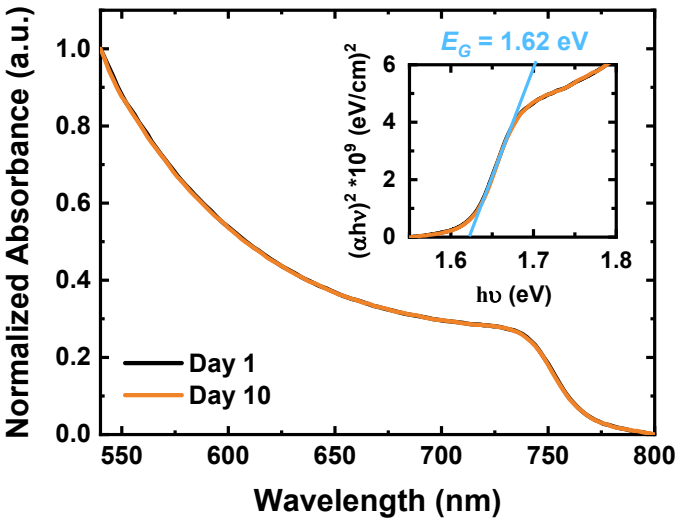

Fig. S10. Normalized absorbance of a perovskite thin film. Normalized absorbance of a $Cs_{0.1}(FA_{0.83}MA_{0.17})_{0.9}Pb(I_{0.83}Br_{0.17})_3$ thin film, characterized on the day of sample preparation (day 1) and after storage (day 10). Inset: Direct optical bandgap (E_G) of the perovskite thin film determined by the Tauc plot for days 1 and 10 (both equal to 1.62 eV).

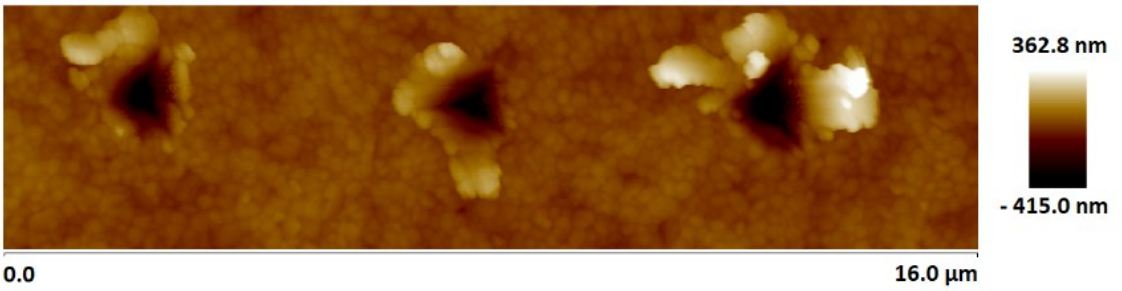

Fig. S11. Atomic force microscopy (AFM) image of three indentations on the surface of a perovskite thin film. We use a diamond AFM tip to indent the surface of the perovskite thin films in order to find an exact examined spot on the same sample on different days of measurements.

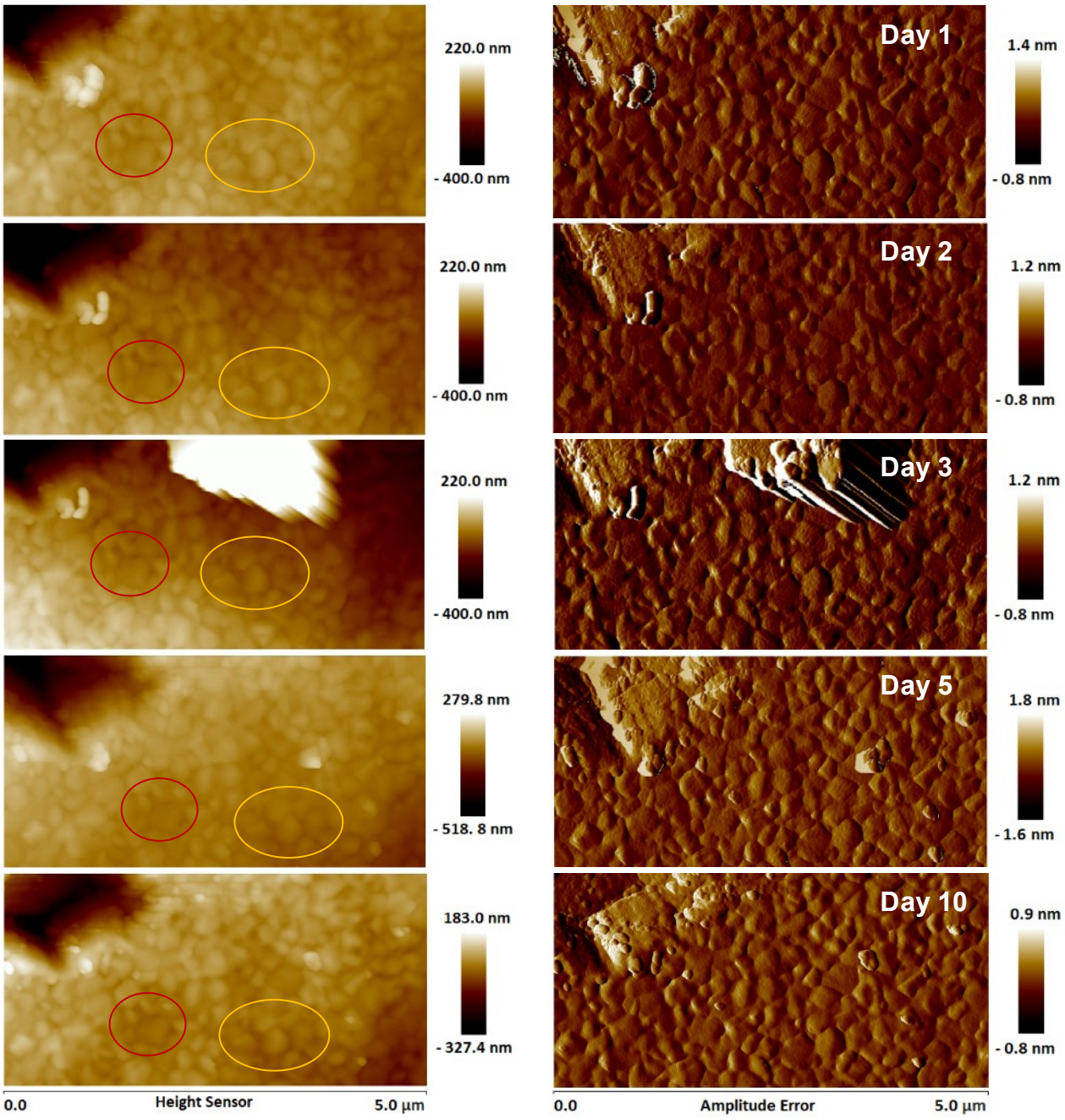

Fig. S12. Atomic force microscopy (AFM) images of the surface of a perovskite thin film. We scan the exact same spot of a $Cs_{0.1}(FA_{0.83}MA_{0.17})_{0.9}Pb(I_{0.83}Br_{0.17})_3$ thin film deposited on glass/ITO/TiO_2 nanoparticles on different days. Left column: The data of the height sensor, containing information of the surface topography of the sample. Right column: The amplitude error, shown for a better illustration of the contrast. The roughness of the layer is ~18.4 nm with no considerable changes on different days.

Table S2. Crystallographic parameters extracted from an XRD pattern of a $Cs_{0.1}FM_{0.9}$ perovskite thin film, comparing days 1 and 5.

Storage Time	Day 1	Day 5	Day 10
Diffraction angle of (001)	14.165°	14.231°	14.301°
Diffraction angle of (002)	28.466°	28.529°	28.599°
d-spacing of (001) [a)]	6.247 Å	6.218 Å	6.188 Å
d-spacing of (002)	6.221 Å	6.206 Å	6.191 Å
Mean d-spacing	6.234 Å	6.213 Å	6.189 Å
Error: d(001)-d(002)	0.026 Å	0.012 Å	-0.0024 Å [b)]
Relative Strain [c)]	0.73%	0.39%	0.00%
FWHM	0.090193°	0.101353°	0.0886624°
Crystallite Size [d)]	128 nm	103 nm	89 nm

[a)] We calculate the d-spacing of the perovskite reflections using Bragg equation:

$$2dsin\theta = n\lambda, \; n = \sqrt{h^2 + k^2 + l^2}$$

[b)] Negative value is due to the fact that we cannot split the peaks in the XRD pattern of day 10.

[c)] We calculate the relative strain of days 1 and 5 normal to (001) using the following equation:

$$\epsilon_r = \frac{\Delta d}{d} = \frac{d_{strained} - d_{unstrained}}{d_{unstrained}}$$

$d_{strained}$ is the mean *d*-spacing of the strained sample on day 1 and $d_{unstrained}$ is the mean *d*-spacing of an unstrained sample on days 5 and 10.

[d)] We calculate the crystallite sizes using the Scherrer equation:

$$D = \frac{K\,\lambda}{\beta \cos\theta}$$

where D is the crystallite size, λ is the wavelength of the X-rays, β is the FWHM in radians, θ is the Bragg angle, and K is the scale factor depending on the shape of the grains. This equation is not valid for crystallite sizes that are too large or too small.

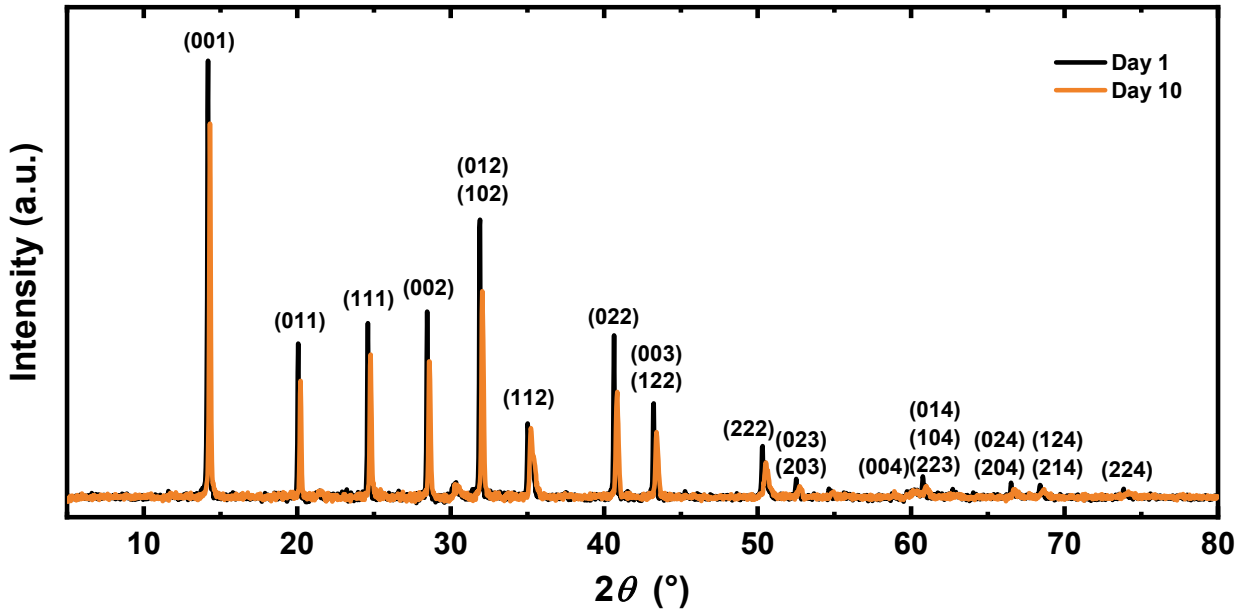

Figure S13. X-ray diffraction (XRD) patterns of the perovskite thin film deposited on SnO_2 collected on the day of sample preparation (day 1) and after storage (day 10). The relative intensities of the reflections for perovskite diffraction patterns collected on different day (before and after dark storage) remain consistent.

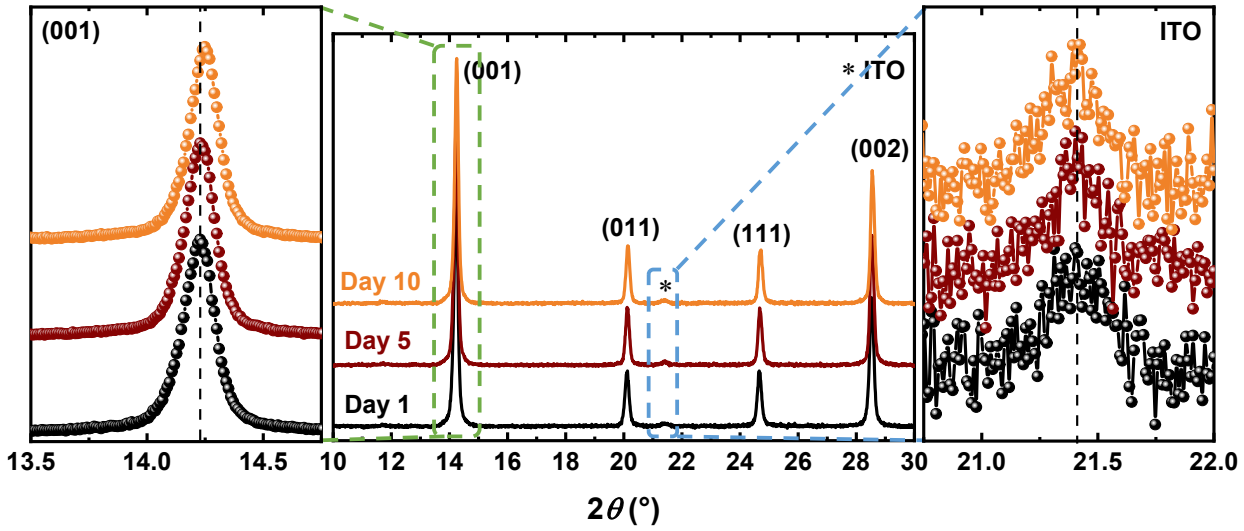

Fig. S14. X-ray diffraction (XRD) patterns for a perovskite thin film collected on different days. All XRD patterns are normalized to (001) perovskite peaks. The composition of the perovskite thin film deposited on glass/ITO/TiO_2 nanoparticles is $Cs_{0.1}(FA_{0.83}MA_{0.17})_{0.9}Pb(I_{0.83}Br_{0.17})_3$. We collect the XRD data on the day of sample preparation (day 1) and after storage (days 5 and 10). Left panel: shift of (001) perovskite peak to higher diffraction angles over time. Right panel: ITO peak at $2\theta = 21.4°$ as a reference.

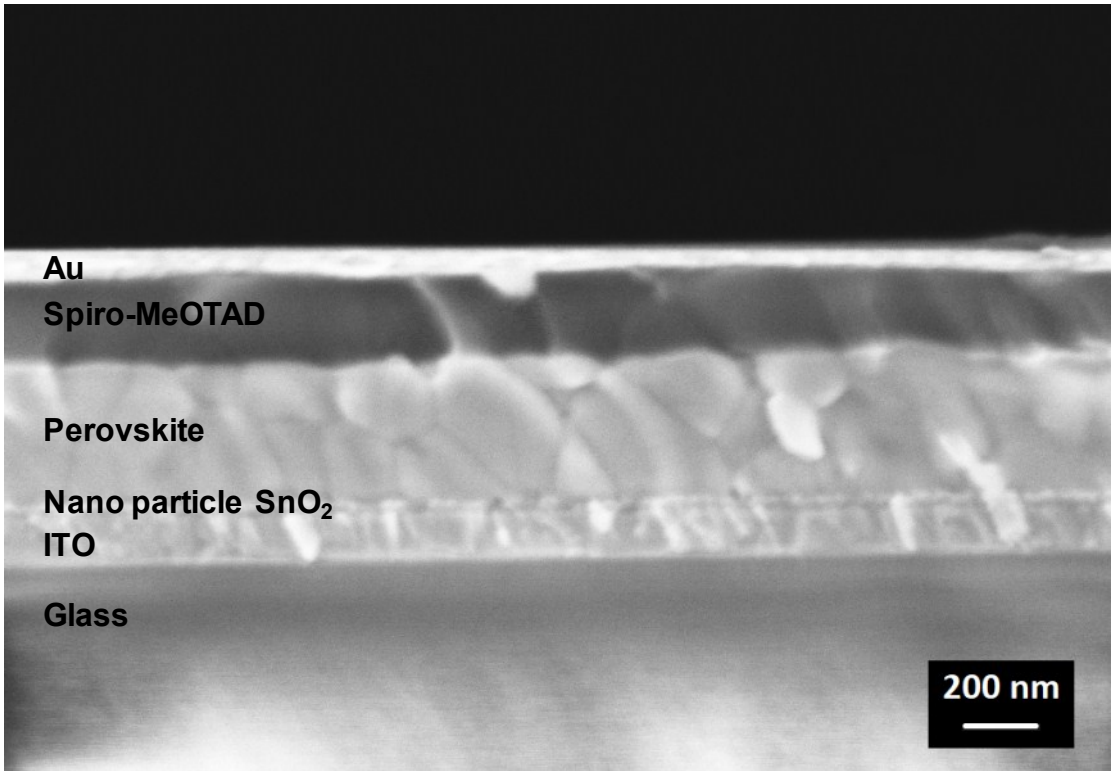

Fig. S15. Cross-sectional scanning electron microscopy (SEM) image of a perovskite solar cell. The layer sequence of the perovskite solar cell is glass/ITO/SnO_2 nanoparticeles/$Cs_{0.1}(FA_{0.83}MA_{0.17})_{0.9}Pb(I_{0.83}Br_{0.17})_3$/spiro-MeOTAD/Au. The perovskite thin film has a thickness of ~370 nm.